Author/s:
Samim, S;Dalton, H;Phillips, D;Hergt, J

Title:
High-resolution tephrochronology resolves stratigraphic complexities in archaeologically significant Nariokotome tuffs, Turkana Basin

Date:
2025-09-23

Citation:
Samim, S., Dalton, H., Phillips, D. & Hergt, J. (2025). High-resolution tephrochronology resolves stratigraphic complexities in archaeologically significant Nariokotome tuffs, Turkana Basin. Proceedings of the National Academy of Sciences of the United States of America, 122 (38), pp.e2424142122-. https://doi.org/10.1073/pnas.2424142122.

PNAS RESEARCH ARTICLE | EARTH, ATMOSPHERIC, AND PLANETARY SCIENCES OPEN ACCESS

High-resolution tephrochronology resolves stratigraphic complexities in archaeologically significant Nariokotome tuffs, Turkana Basin

Saini Samim[a,1], Hayden Dalton[a], David Phillips[a], and Janet Hergt[a]

Affiliations are included on p. 12.

Edited by Thure Cerling, The University of Utah, Salt Lake City, UT; received November 25, 2024; accepted August 8, 2025

The Turkana Basin is a renowned paleoanthropological region in Kenya and Ethiopia and is famous for discoveries of numerous hominin fossils and their associated cultural technologies. The Plio-Pleistocene sedimentary sequences hosting these important remains are interbedded with volcanic ash (tuff) beds that provide crucial bracketing age constraints. The Nariokotome Tuff Complex, comprising the Upper, Middle, and Lower Nariokotome Tuffs, preserves deposits that cover an important time interval during the late Early Pleistocene that saw milestone events for *Homo erectus* and associated technological development. Unfortunately, characterization of these tuffs has been hampered by a) overlapping published eruption ages and b) indistinguishable major element compositions. In addition, fluvial reworking of feldspar-bearing pumice clasts (the target rock for age determinations) from older volcanic deposits into younger tuff layers complicates correct age assignments. Here, we use multiple tephrochronological correlation tools, including high-resolution ^{40}Ar/^{39}Ar geochronology and grain-specific major- and trace-element geochemistry, to establish a well-characterized geochemical and geochronological framework for the Nariokotome tuffs. Utilizing a modern-generation mass-spectrometer, we report distinct ages for the Upper Nariokotome Tuff at 1,233.1 ± 1.3 ka (± 1.9 ka, 2σ; including external uncertainties), the Middle Nariokotome Tuff at 1,263.4 ± 1.2 ka (± 1.9 ka) and the Lower Nariokotome Tuff at 1,285.8 ± 1.0 ka (± 2.1 ka). In addition, high-spatial resolution Laser Ablation Inductively Coupled Mass Spectrometry trace element compositions provide distinct characterization of each tuff, aiding intrabasin correlation of these units. This combined methodology demonstrates the potential to resolve the stratigraphic complexities associated with assigning ages to key paleoanthropological sites.

Turkana Basin | hominin | high-precision ^{40}Ar/^{39}Ar geochronology | tephrochronology | Nariokotome tuffs

Significance

The Nariokotome Tuff Complex in the Turkana Basin, Kenya, hosts rare late Early Pleistocene paleoanthropological sites crucial for understanding *Homo erectus* and their associated cultural technology, highlighted by decades of remarkable discoveries. These important artifacts interbedded with volcanic ash (tuffs), offer valuable age constraints for fossiliferous horizons. However, distinguishing these tuffs has been problematic due to overlapping ages and similar major element compositions. Using high-precision tephrochronological techniques, including high-resolution ^{40}Ar/^{39}Ar geochronology and Laser Ablation Inductively Coupled Mass Spectrometry (LA-ICP-MS) trace-element analysis, we resolve these challenges by establishing distinct ages and geochemical fingerprints for the Upper, Middle, and Lower Nariokotome Tuffs. This refined stratigraphy provides tighter age constraints for key paleoanthropological sites and strengthens the tephrostratigraphic framework within and beyond the Turkana Basin.

Voluminous ash fall deposits ([*] tuff layers) serve as important chronostratigraphic markers in establishing the timescales of sedimentary records (1, 2). The Omo Group is a Plio-Pleistocene volcano-sedimentary succession located in the Turkana Basin, NW Kenya, and SW Ethiopia (Fig. 1*A*), and is hosted within the East African Rift System (EARS) (3–7). The Omo Group has been extensively studied due to the presence of several important hominin species [e.g., *Homo, Paranthropus*; (8)], their cultural technology (9, 10) and numerous interbedded tuff layers that provide bracketing age constraints for these important horizons (3–5, 11–13). The presence of these widespread tuffs, which are important lithostratigraphic marker beds, also form the basis for correlating temporally equivalent strata within the Turkana Basin and across other formations within the EARS. The key to gaining a regional perspective of these important fossiliferous horizons lies in building a robust tephrostratigraphic and tephrochronological framework.

The Omo Group comprises three primary formations and outcrop areas: the Shungura Formation in the north, the Koobi Fora Formation in the east and the Nachukui Formation in the west of Turkana Basin (15; Fig. 1 *A–C*). Temporal equivalence of these formations (tephrochronology) within the Turkana Basin has been established primarily through geochemical analyses [major and minor elements by electron probe microanalysis (EPMA); select major, minor, and trace elements by X-ray fluorescence analysis (XRF)] of volcanic

---

[*] A tuff is a sedimentary deposit that is primarily composed of volcanic ash particles. Other components in a tuff may include juvenile clasts (e.g., pumice clasts that may contain fresh crystals suitable for radiometric dating), reworked sediments and detrital minerals.

This article is a PNAS Direct Submission.

PNAS policy is to publish maps as provided by the authors.

[1] To whom correspondence may be addressed. Email: saini.samim@unimelb.edu.au.

This article contains supporting information online at https://www.pnas.org/lookup/suppl/doi:10.1073/pnas.2424142122/-/DCSupplemental.

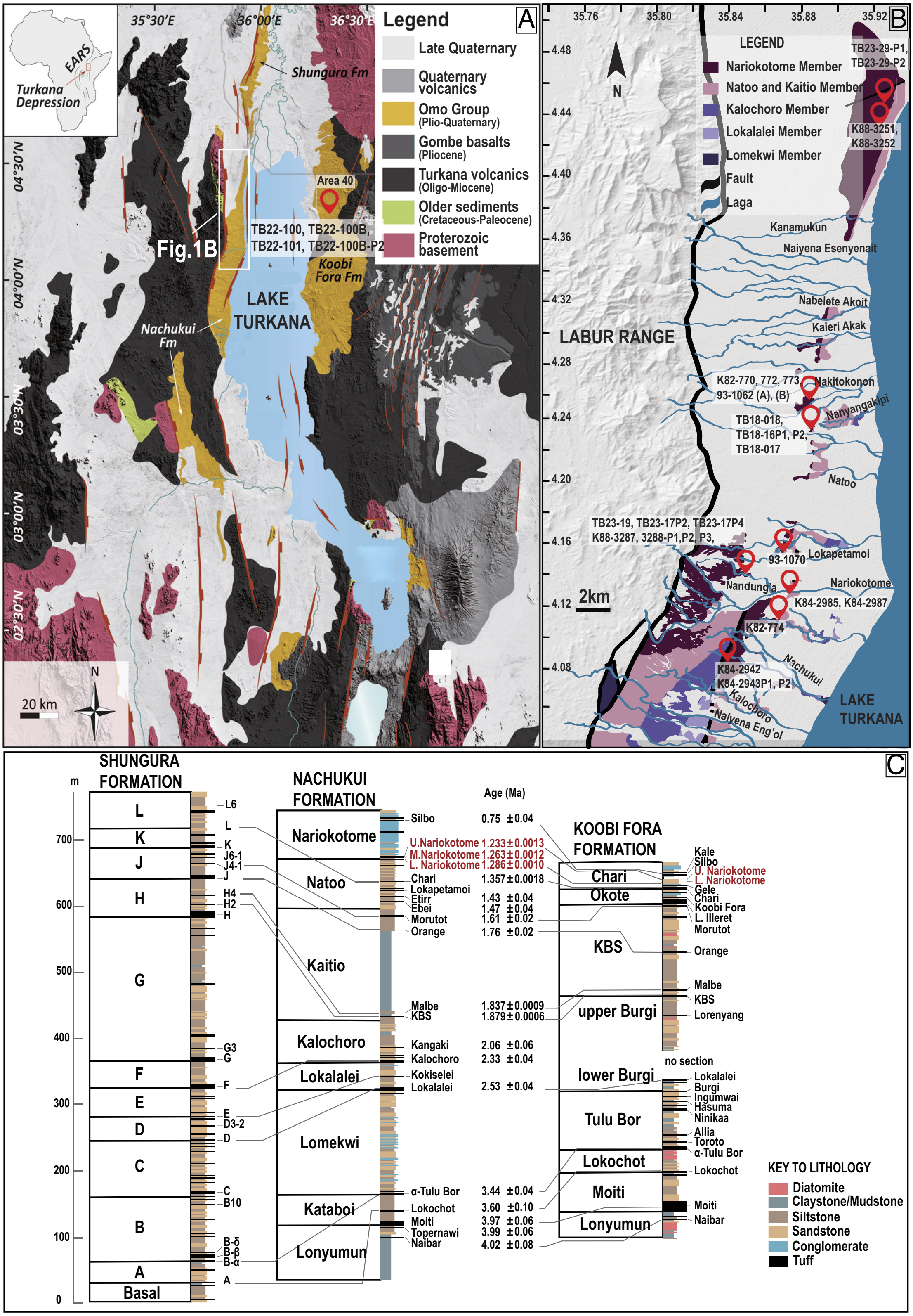

Fig. 1. Locality map of the Turkana Basin and the Nachukui Formation. (*A*) Location map of the Turkana Basin, hosted within the EARS [modified from Nutz, Schuster, Boës, and Rubino (14)]. The yellow units show the three temporally equivalent sedimentary successions that form the Omo Group, the Shungura Formation in the north, Koobi Fora Formation in the east and Nachukui Formation in the west [modified after McDougall and Brown (4)]. (*B*) Locality map of the Nachukui Formation showing the different members and localities of samples used in this study [modified from Nutz, Schuster, Boës, and Rubino (14)], (*C*) Stratigraphic sections of the Shungura, Nachukui, and Koobi Fora formations (modified from McDougall et al. (13)). Ages reported in the stratigraphic section (black text) have been compiled from McDougall and Brown (4), McDougall and Brown (3), and Phillips et al. (12) are reported at the ±2σ level. Ages in red text relate to those produced in this study.

glass shards from the tuff units (5, 16–18). Pumice clasts found enclosed in the tuff layers have also been routinely utilized to ensure the comagmatic origin of the pumice clasts and tuff layers from an individual eruption (3, 5, 13). However, volcanic centers within the central sector of the Main Ethiopian Rift (MER), speculated as the source volcano(es) for Turkana Plio-Pleistocene tuffs, are known to produce tuff layers exhibiting similar major and minor element geochemistry (19–22). This has hindered both the identification and correlation of tuff units within Turkana Basin and made it difficult to identify their source volcanic centers. High-resolution grain-specific, Laser Ablation Inductively Coupled Mass Spectrometry (LA-ICP-MS) trace element geochemistry on tuff and pumice glass has shown the potential of "fingerprinting" eruptions with distinct trace element geochemistry (23), but remains to be widely implemented in the Turkana Basin. Previous geochronology in the Turkana Basin has been largely obtained through ^{40}Ar/^{39}Ar dating of feldspar grains collected from pumice clasts that are found within the tuff layers (3–5, 24). Unfortunately, the large analytical uncertainties (25 to 30 ka, 1σ) associated with most published eruption ages means that many closely spaced tuff layers are temporally indistinguishable (13). Recent work on tuffs of the Turkana Basin, has shown the potential of utilizing ultra-high-precision ^{40}Ar/^{39}Ar geochronology to distinguish closely spaced eruptions and hence provide tighter age constraints (uncertainties on the order of 1 to 2 ka, 2σ) for tuff layers and associated paleontological/archaeological materials (12). Furthermore, with increased analytical precision of modern mass spectrometers, crystal ages older than the "true" eruption ages have been increasingly recognized in silicic systems, which has warranted the application of a Bayesian statistical approach after Keller, Schoene, and Samperton (25) for estimating an eruption age, rather than the traditional arithmetic or weighted mean approach (12, 26, 27). A comprehensive tephrochronological framework, based on high-resolution geochronology and trace element geochemistry, therefore has the potential to provide insights into providing temporal and geochemical "fingerprints" between closely spaced tuff units to aid intra- and interbasin correlation of paleoanthropologically rich regions throughout East Africa.

This study focuses on three of the youngest paleoanthropologically significant tuffs in the Turkana Basin; the Upper Nariokotome (UNK), Middle Nariokotome (MNK), and Lower Nariokotome (LNK) Tuffs, collectively referred to as the Nariokotome tuffs (6, 28). We utilize two key tephrochronological tools: 1) ultra-high-precision ^{40}Ar/^{39}Ar geochronology on single feldspar grains, and 2) grain-specific major and trace element geochemistry of pumice glass and tuff glass shards, in order to constrain the temporal and geochemical characteristics of the Nariokotome units.

1.1. The Nariokotome tuffs. The UNK, MNK, and the LNK Tuffs are closely spaced volcanic ash layers that occur within the youngest member, the Nariokotome Member, of the Nachukui Formation (Fig. 1 *B* and *C*; 4, 28). These three sequential, vitric layers are interbedded with volcaniclastic conglomerates, sandstones, and siltstones in a ca. 7 m thick complex, locally referred to as the Nariokotome Tuff Complex. The Nariokotome Member is defined by the base of the LNK Tuff; the LNK Tuff is an important local marker layer that is used for correlations within the Nachukui Formation (6, 13, 28), and also forms an important age constraint for late Early Pleistocene fossils/artifacts (6, 11, 28–32). In addition, the Nariokotome tuffs, along with the Silbo Tuff, (Fig. 1*C*) are the only temporal anchor points to constrain paleoclimate models during the Middle Pleistocene Transition; the time period wherein glacial/interglacial cycles changed their dominant frequencies from ~40 kyrs to ~100 kyrs (33).

The predominant mineral phase in the pumice clasts from the Nariokotome tuffs is alkali feldspar, but minor amounts of quartz are also present in pumice clasts from the LNK Tuff. Previous studies of the Nariokotome tuffs have mainly focused on determining their tuff glass geochemistry and eruption ages for the purpose of basin-wide (e.g., Nachukui and Koobi Fora Formation) and interbasin correlations (e.g., Usno and Konso Formation) (4–6, 13, 21, 28, 34–36). Various attempts have been made to characterize the Nariokotome tuffs geochemically. Published major element geochemical compositions for the three Nariokotome tuffs, however, are largely indistinguishable. The major and minor element geochemistry of the Nariokotome tuffs have been reported to show that only the LNK Tuff is compositionally distinct (28), whereas the MNK and UNK Tuffs are very similar (4). Unfortunately, published geochemical datasets are incomplete and are limited to either averages or representative analyses. In addition, published ^{40}Ar/^{39}Ar eruption ages of the Nariokotome tuffs are also indistinguishable. The LNK Tuff has an eruption age of 1,298 ± 50 ka (2σ) (4). ^{40}Ar/^{39}Ar age estimates of the MNK and UNK Tuffs are only slightly younger than the LNK Tuff, at 1,277 ± 60 (2σ) and 1,230 ± 40 ka (2σ), respectively (4). These age estimates are arithmetic simple mean ages and are widely used in the literature for interpreting associated fossil/artifact ages (e.g., refs. 11, 29, and 37). The corresponding weighted mean ages from McDougall and Brown (4) are comparatively precise at 1,236 ± 12 ka (2σ), 1, 295 ± 19 ka (2σ), 1, 304 ± 9 ka (2σ) for the UNK, MNK, and LNK Tuffs respectively; however, the weighted mean age estimates for the MNK and LNK Tuffs are also indistinguishable The widespread nature of the Nariokotome tuff layers and the lack of geochemical and temporal identification necessitates a new approach for fingerprinting these tuffs.

2. Results

2.1. Major And Trace Element Geochemistry.

2.1.1. Pumice and tuff glass geochemistry.

2.1.1.1. Upper Nariokotome Tuff. Pumice and tuff glass shards from the UNK Tuff display a unimodal signature with low total Fe as Fe^{+2} (FeO$_T$) (3.4 to 3.9 wt%), moderate Al$_2$O$_3$ (9.9 to 10.9 wt%) and moderate TiO$_2$ (0.2 to 0.3 wt%) contents (Fig. 2*A* and *SI Appendix*, Fig. S1*A*). In terms of incompatible trace element geochemistry, absolute abundances of Ti and Ba (Fig. 2*B*) and select trace elemental ratios e.g., Ti/Zr vs Ba/Nb, La/Nb vs Ba/Zr (Fig. 2*D* and *SI Appendix*, Fig. S1*D*) are useful for discriminating the UNK Tuff (Fig. 2 *B*–*D*). UNK pumice and tuff glass trace element geochemistry is characterized by distinctive Ba (~390 to 430 ppm, Fig. 2*B*) and Ti (~1,280 to 1,450 ppm, Fig. 2*B*), and notable incompatible trace elemental abundances such as La and Zr (La: ~100 to 115m ppm, Zr: ~950 to 1,050 ppm; Fig. 2*C*), which are useful in tuff identification. In primitive-mantle normalized and chondrite-normalized diagrams (*SI Appendix*, Fig. S2*A*), the UNK glasses display slight depletion in Ba, pronounced depletions in Sr and Ti, and Eu/Eu* = ~0.55.

2.1.1.2. Middle Nariokotome Tuff. The MNK pumice and tuff glass shards show a bimodal signature with two distinct clusters in major and trace element geochemistry. These clusters are termed Mode 1, which has a less evolved composition (i.e., higher Fe and Ca, and lower incompatible trace element contents), and Mode 2, which exhibits a comparatively more evolved composition.

The Mode 1 composition is characterized by higher concentrations of FeO$_T$ (3.8 to 4.5 wt%), Al$_2$O$_3$ (10.7 to 11.5 wt%) (Fig. 2*A*) TiO$_2$ (0.3 to 0.4 wt%) and CaO (0.35 to 0.45 wt%) (*SI Appendix*, Fig. S1 *A* and *B*) compared to the Mode 2 composition described below. In terms of absolute trace element abundances, Mode 1 samples exhibit lower concentrations of Large Ion Lithophile Elements (Fig. 2*B*), Rare Earth Elements (REE; e.g., La: ~85 to 95 ppm; Fig. 2*C*), and High Field Strength Elements (e.g., Zr: ~700 to 800 ppm; Fig. 2*C*). The Mode 2 composition is geochemically similar to (and overlaps with) the UNK pumice

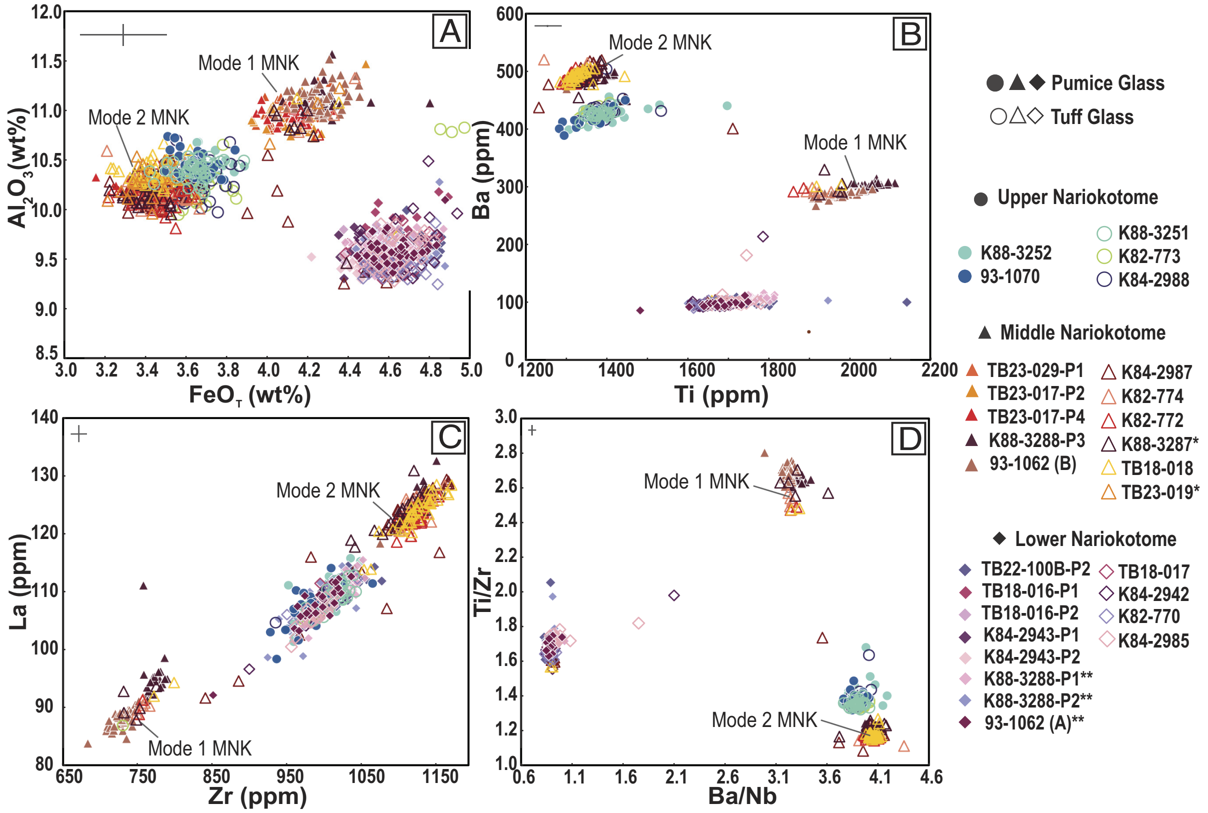

Fig. 2. Scatterplots displaying major element oxide concentrations (in wt%) and trace element concentrations (in ppm) of pumice and volcanic glass shards from the three Nariokotome tuffs. (*A*) Al_2O_3 vs. FeO_T, (*B*) Ti vs. Ba, (*C*) La vs. Zr, (*D*) Ti/Zr vs. Ba/Nb. Error bars represent % RSD values obtained by analyzing matrix-matched rhyolitic glass standards, VG-568 (n = 31, for major element oxides concentrations) and the trace element reference ATHO-G (and are plotted on the top left corner of each panel. The asterisk (*) indicates tuff samples previously misidentified/unidentified due to similar MNK (Mode 2) and UNK major element geochemistry but now correctly identified as MNK applying major and trace element geochemistry. Double asterisk (**) indicates previously unidentified LNK pumice samples reworked into the younger MNK Tuff layer.

and tuff glass major element geochemical composition and exhibits lower FeO_T (3.1 to 3.7 wt%), Al_2O_3 (9.9 to 10.6 wt%) (Fig. 2*A*), TiO_2 (0.2 to 0.3 wt%) and CaO (0.18 to 0.28 wt%) contents (*SI Appendix*, Fig. S1 *A* and *B*). With respect to trace element abundances, Mode 2 samples can be readily distinguished from the UNK glass geochemistry by their higher abundances of most incompatible trace elements (e.g., La and Zr; Fig. 2 *B* and *C*).

It is important to note that individual MNK pumice clasts are dominated by Mode 1 compositions and Mode 2 compositions are less common. In contrast, MNK Tuff glass shards from individual samples are dominated by Mode 2 compositions and Mode 1 compositions are rare (Fig. 2 *A–D*). Moreover, the bimodal composition of the MNK glass geochemistry persists in primitive-mantle normalized spider diagrams, with the negative Ba anomaly more pronounced in Mode 1 relative to Mode 2 samples, which is again indistinguishable from the UNK Tuff (*SI Appendix*, Fig. S2*A*). The average MNK Tuff and pumice glasses also display the smallest negative Eu anomaly; with MNK pumice (Mode 1) Eu/Eu*= ~0.5, and Mode 2 Eu/Eu* = ~0.6 (*SI Appendix*, Fig. S2*B*).

2.1.1.3. Lower Nariokotome Tuff. Of the three Nariokotome tuffs, pumice and tuff glass shards from the LNK Tuff display a unimodal major element geochemistry distinct from UNK and MNK compositions, with the highest FeO_T (4.3 to 4.9 wt%), lowest Al_2O_3 (9.2 to 9.8 wt%), and moderate TiO_2 (0.25 to 0.35 wt%) contents (Fig. 2 *A–C*). With the exception of Ti and Ba, the trace element abundances of LNK pumice clasts and tuff glasses overlap those of the UNK glass compositions. Pb elemental abundances for UNK and LNK samples have considerable overlap, but LNK glasses tend toward higher Pb abundances, as exemplified by the offset between the geochemical clusters for LNK and UNK glass chemistries (*SI Appendix*, Fig. S1*C*). The LNK Tuff is best distinguished from the other tuffs using Ti and Ba elemental abundances and trace element ratios involving Ti and Ba (e.g., Ba/Nb, Ba/Zr, Ti/Zr; Fig. 2 *B* and *D*). The LNK glass geochemistry exhibits the most pronounced negative Ba anomaly and a less pronounced positive Pb anomaly (*SI Appendix*, Fig. S2*B*) compared with the other tuffs. It is also important to highlight that sample 93-1062A was collected from an MNK Tuff layer (4), but both major and trace element signatures indicate that this sample is an LNK pumice (Fig. 2 *A–D* and discussed further in Section 3.3.1).

In summary, on the basis of the major element geochemistry of tuff and pumice glass samples, these three units are best distinguished by their Al_2O_3, FeO_T, and TiO_2 contents (Fig. 2*A* and *SI Appendix*, Fig. S1*A*), as there is considerable overlap for other major oxides (*SI Appendix*, Fig. S1*B*). Even so, the bimodal compositions preserved in samples from the MNK Tuff result in considerable overlap between the UNK and Mode 2 MNK samples and cannot be distinguished based on major element geochemistry of tuff glasses alone. Trace element abundances and ratios, however, are distinctive and useful for identification of these tuffs. A summary table outlining the average major element oxide contents and trace element concentrations for the three Nariokotome tuffs, including the two compositional modes of the MNK Tuff, is provided in *SI Appendix*, Table S2 and *SI Text*, *Extended Methods*.

2.1.2. Feldspars. The feldspar grains from each of the three tuff units, UNK, MNK, and LNK Tuffs define a tight compositional range in the anorthoclase field, (Fig. 3 *A–C*), and occur as three clusters in major element space (Fig. 3 *D–F*). Feldspar compositions from LNK pumice clasts can be readily distinguished on the basis of their major element composition, whereas the feldspar crystals from

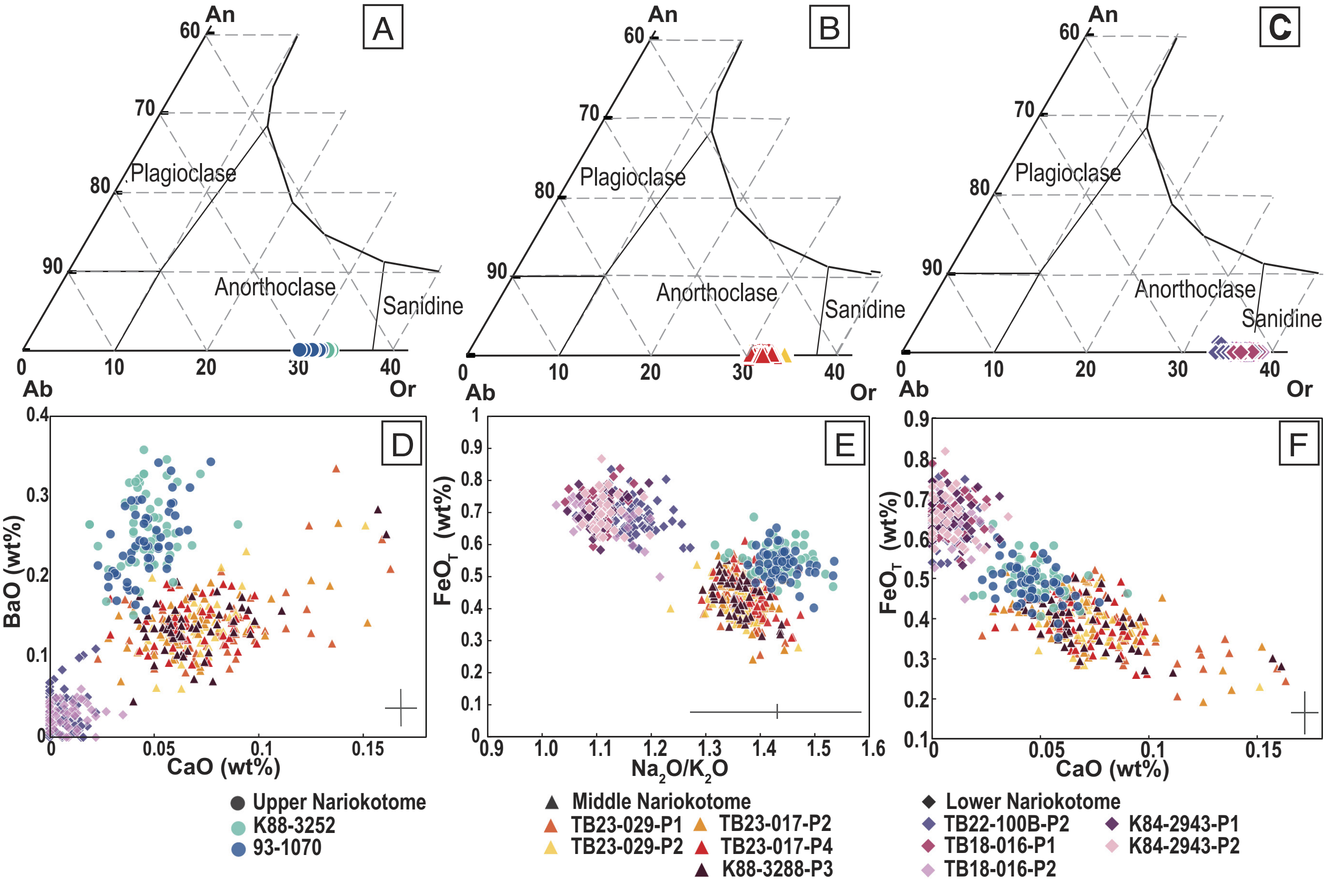

Fig. 3. Major element geochemistry of single feldspar crystals from the Nariokotome tuffs. (*A*–*C*) Ternary diagrams displaying the feldspar geochemical composition for the UNK (*A*), MNK (*B*), and LNK (*C*) pumice clasts wherein end-member compositions are represented by An = Anorthite, Ab = Albite and Or = Orthoclase. (*D*–*F*) Scatterplots displaying the major element oxide contents (in wt%) of feldspars from the three Nariokotome tuffs. (*D*) BaO vs. CaO (*E*) FeO$_T$ vs. Na$_2$O/K$_2$O and (*F*) FeO$_T$ vs. CaO. Error bars represent % RSD obtained by analyzing matrix-matched rhyolitic glass standards, VG-568 (*n* = 24), for major element oxide contents) and are plotted on the bottom right corner of each panel.

UNK and MNK pumices (confirmed identities from pumice glass chemistry) exhibit broadly similar ranges with some overlap (Fig. 3 *D*–*F*). UNK anorthoclase (Or$_{0.30}$ – Or$_{0.33}$; Fig. 3*A*) typically exhibits higher and more restricted BaO (0.15 to 0.35 wt%; Fig. 3*D*) and CaO contents (0.03 to 0.06 wt%; Fig. 3 *D* and *F*) and higher FeO$_T$ contents (0.40 to 0.69 wt%; Fig. 3 *E* and *F*) relative to MNK and LNK. MNK feldspars display marginally broader anorthoclase compositions (Or$_{0.30}$ – Or$_{0.34}$; Fig. 3*B*), lower and variable BaO contents (0.04 to 0.34 wt%; Fig. 3*D*), the highest CaO (0.04 to 0.15 wt%; Fig. 3 *D* and *F*), and lower FeO$_T$ contents (0.24 to 0.61 wt%; Fig. 3 *E* and *F*). Feldspar compositions from LNK pumice clasts plot close to the anorthoclase – sanidine boundary, (Or$_{0.33}$ – Or$_{0.39}$; Fig. 3*C*), display the lowest BaO (0 to 0.11 wt%; Fig. 3*D*), lowest CaO (<0.02 wt%, Fig. 3 *D* and *F*), and highest FeO$_T$ contents (0.49 to 0.86 wt%; Fig. 3 *E* and *F*).

2.2. ^{40}Ar/^{39}Ar High-Resolution Geochronology.

^{40}Ar/^{39}Ar geochronological analyses conducted on individual feldspar crystals yielded a range in apparent ages for individual pumice clasts collected from a single tuff unit. Consequently, eruption ages were estimated using the Bayesian statistical approach of ref. 25 (*Materials and Methods* and *SI Appendix*, *SI Text*). These results are summarized below (and in *SI Appendix*, Fig. S3 *A*–*C* and Table S3), and full datasets are presented in Datasets S7 and S8 (38).

2.2.1. *Upper Nariokotome Tuff.* ^{40}Ar/^{39}Ar data were obtained from a total of 58 individual feldspar crystals from two UNK pumice clasts (samples K88-3252, 93-1070, *SI Appendix*, Fig. S3*A*). Analysis of 32 single feldspar crystals from sample K88-3252 show an age distribution ranging from 1,231.5 ± 1.3 to 1,289.6 ± 1.6 ka spanning 58.1 ± 2.0 ka (all ages are reported with 2σ uncertainty unless stated otherwise). Similarly, ages for 24 feldspar crystals from sample 93-1070 range from 1,228.7 ± 2.2 to 1,290.8 ± 0.8 ka, spanning 62.1 ± 2.3 ka. Bayesian eruption age estimates calculated for these two pumice clasts are 1,232.7 ± 1.6 ka and 1,233.5 ± 2.4 ka, respectively (*SI Appendix*, Fig. S3*A* and Table S3). No obvious correlation between Ca/K ratios and age was observed (Dataset S7).

The weighted-mean age for the two Bayesian estimates [calculated using Isoplot; 39] is 1,232.9 ± 1.3 ka (MSWD = 0.31, *P* = 0.58) (Fig. 4). The Bayesian eruption age estimate for the combined dataset (*n* = 56 feldspars) from the two UNK pumice clasts is 1,233.1 ± 1.3 ka, indistinguishable from the intersample weighted mean age for UNK (Fig. 4).

2.2.2. *Middle Nariokotome Tuff.* Single feldspar crystals (*n* = 157) from six MNK pumice clasts (samples TB23-029-P1, TB23-029-P2, TB23-017-P2, TB23-017-P4, 93-1062B, K88-3288-P3) were analyzed, yielding ^{40}Ar/^{39}Ar apparent ages ranging from 1,259.4 ± 5.5 to 1,420.7 ± 3.1 ka, spanning 161.3 ± 6.3 ka. Bayesian eruption age estimates for five individual pumice clasts provide concordant results (*SI Appendix*, Fig. S3*B*) of 1,262.6 ± 2.6 ka (sample TB23-029-P1), 1,264.6 ± 1.9 ka (sample TB23-029-P2), 1,262.5 ± 2.4 ka (sample TB23-017-P4), 1,262.6 ± 2.6 ka (sample 93-1062B) and 1,263.4 ± 5.9 ka (sample K88-3288-P3) (*SI Appendix*, Fig. S3*B* and Table S3). A single pumice clast, TB23-017-P2 yields a marginally older Bayesian age estimate of 1,271.4 ± 2.7 ka (*SI Appendix*, Fig. S3*B*). No obvious correlations between Ca/K and ages were observed (Dataset S7).

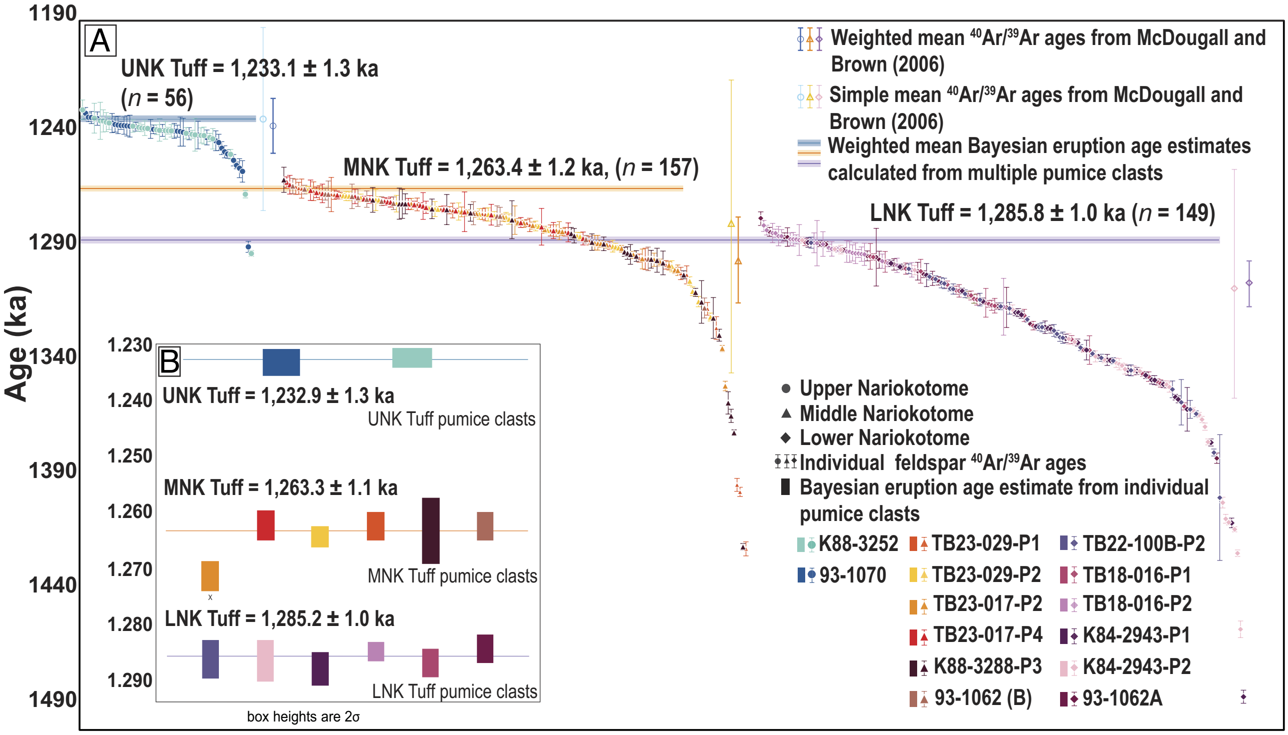

Fig. 4. Summary age diagram of $^{40}Ar/^{39}Ar$ ages from the three Nariokotome tuffs. (*A*) Summary age diagram of $^{40}Ar/^{39}Ar$ ages of individual feldspar grains from multiple pumice clasts from the three Nariokotome tuffs. Error bars on individual $^{40}Ar/^{39}Ar$ ages represent 2σ analytical uncertainties. Our preferred Bayesian age estimates for the tuffs (excluding external uncertainties) are represented as horizontal blue, yellow, and purple bars. The Bayesian age estimates were calculated for individual pumice clasts (shown in the subset figure *B*) and the final Bayesian age estimate reported for each tuff is the weighted mean calculated from multiple pumice clasts within subset *B*. Composite Bayesian ages (preferred ages) for each tuff are represented in *A*. Arithmetic mean ages and weighted mean ages (with 2σ uncertainties) for the Nariokotome tuffs from previous study (4) have been recalculated to our preferred FCTs monitor age and decay constant, for comparison with results from this study. Note that sample TB23-17P2 is excluded from the final age calculation for the MNK Tuff.

The weighted-mean age estimates for all six MNK pumice clasts is 1,264.6 ± 3.5 ka (2σ, MSWD = 6.9, P = <0.01). The precision of this estimate improves to 1,263.3 ± 1.1 ka (MSWD = 0.73 P = 0.57), if the older sample (TB23-017-P2) is excluded from the weighted mean calculation (Fig. 4). Irrespective of inclusion of this sample, the composite (n = 157) Bayesian approach gives an eruption age estimate of 1,263.4 ± 1.2 ka, which is indistinguishable from the weighted intersample (n = 5) Bayesian age for the MNK Tuff (Fig. 4).

2.2.3. Lower Nariokotome Tuff. Feldspar crystals (n = 155) from six LNK pumice clasts (samples TB18-016-P1, TB18-016-P2, K84-2943-P1, K84-2943-P2, 93-1062A, TB22-100B-P2) display the most positively skewed $^{40}Ar/^{39}Ar$ age distribution of all three tuffs, ranging from 1,276.4 ± 3.0 ka to 1,485.8 ± 3.0 ka, spanning a total of 209.4 ± 4.2 ka (*SI Appendix*, Fig. S3*C*).

Bayesian eruption age estimates for four of the six pumice clasts are analogous at 1,286.8 ± 2.4 ka (TB18-016-P1), 1,287.5 ± 3.3 ka (K84-2943-P1), 1,285.5 ± 3.6 ka (K84-2943-P2) and 1,287.5 ± 3.2 ka (TB22-100B-P2), respectively (*SI Appendix*, Fig. S3*C* and Table S3). Bayesian eruption age estimates of samples 93-1062A and TB18-016-P2 are slightly younger at 1,277.3 ± 3.9 and 1,281.6 ± 1.9 ka (2σ) respectively (*SI Appendix*, Fig. S3*C*). These two samples show six feldspar crystals with marginally younger ages, not recorded in the other four pumice clasts. Therefore, we excluded the youngest feldspars from these samples (n = 2 and n = 4 from samples 93-1062A and TB18-016-P2) which resulted in more concordant Bayesian age estimates of 1,284.3 ± 2.5 ka and 1,283.6 ± 1.7 ka respectively.

The weighted mean age estimates for all six pumice clasts (excluding the youngest feldspar ages from two samples) is 1,285.2 ± 1.0 ka (MSWD = 1.9, P = 0.087) (Fig. 4 and *SI Appendix*, Table S3). The composite Bayesian age estimate for all LNK pumice clasts (n = 149, excluding the six feldspars grains) is 1,285.8 ± 1.0 ka, which is within the uncertainty of the Bayesian intersample weighted mean age (Fig. 4).

3. Discussion

3.1. Tephra Fingerprinting of the Nariokotome tuffs. The major element data for the three Nariokotome tuffs presented here provide characteristic geochemical fingerprints for the three units (Fig. 2*A* and *SI Appendix*, Fig. S1 *A* and *B*). In the case of the LNK Tuff, the geochemical affinity of LNK pumice clasts with their host LNK Tuff, reaffirms the comagmatic origin of these pumice samples, and is sufficiently distinct to permit the correct discrimination of this horizon. The UNK tuff and pumice clasts glass composition also confirms their comagmatic origin; however, UNK Tuff glass and pumice clasts major element compositions overlap with the dominant Mode 2 composition of the MNK Tuff. The lack of geochemical affinity between the MNK pumice and tuff glasses, both in terms of major and trace element abundances and ratios, raises questions on a comagmatic origin, with Mode 1 and Mode 2 possibly representing the simultaneous eruption of two magmas. Such heterogeneous signatures could imply changes in the magma source or magma chamber processes or both. Possible scenarios could include extraction of magmas from a complex magma body underneath a single volcano or discrete magma bodies beneath separate volcanoes. A detailed investigation to distinguish between these possibilities is an important avenue for future research. Nevertheless, the identification of the bimodal geochemical signatures (Mode 1 and Mode 2) for the MNK Tuff layer and its pumices has not been described in previous studies (4, 28).

Discrimination of the MNK and UNK Tuff layers, therefore, has proven challenging. As noted by McDougall and Brown (4) (see also Fig. 2*A*, this study), there is compositional overlap between the UNK glasses and the dominant tuff glass composition (Mode 2) of the MNK Tuff. The bimodal geochemical signature of the MNK pumice and tuff glass, in addition to the chemically distinct MNK pumice glass (Mode 1) composition, can be utilized as distinguishing factors to identify MNK Tuff layer. A difficulty, however, remains that the bimodal signature within an individual pumice clast/tuff sample for an MNK sample is uncommon and dependent on the number of tuff glass/pumice glass analyses conducted. This means that the Mode 1 composition in the MNK Tuff glass might be overlooked. Hence, the major element geochemistry on its own, is insufficient as a tephrochronological tool for discriminating between the UNK and MNK (Mode 2) Tuffs. In particular, if there is an absence of pumice clasts (which has a distinct major element composition identified as Mode 1) in an MNK Tuff layer, the major element compositions of UNK and the Mode 2 population of MNK tuff glass (Fig. 2*A* and *SI Appendix*, Fig. S1 *A* and *B*) are indistinguishable. This highlights the need for a more reliable discrimination tool.

Based on the combined major and trace element data, we have now identified the key geochemical discriminants for the three Nariokotome tuffs, as summarized in Fig. 2 *A–D*, Table 1, and *SI Appendix*, Fig. S1. For example, even though the bimodality persists in the trace element signature of the MNK tephra products (tuff glass shards and pumice glass), the compositional overlap between the Mode 2 MNK signature and the UNK signature is resolved using trace element abundance data (e.g., La and Zr concentrations in Table 1). In addition, incompatible trace element ratios, such as Ti/Zr vs Ba/Nb (Fig. 2*D*), show tight compositional clusters for each of the three Nariokotome layers. This outcome provides an important example of the utility of trace element fingerprinting as a key tephrochronological tool in the Turkana Basin (Section 3.3).

3.2. Distinct ^{40}Ar/^{39}Ar Ages for the Nariokotome tuffs. As noted above, previously published simple mean ages of the three Nariokotome tuffs are indistinguishable at the 95% confidence level, with simple mean ages of 1,233.3 ± 40 ka (UNK), 1,280.0 ± 64 ka (MNK) and 1,301.8 ± 50 ka (LNK; recalculated from ref. 4; see *Materials and Methods*). The weighted mean ages recalculated from McDougall and Brown (4) are comparatively precise for the three Nariokotome tuffs at 1,236 ± 12 ka (2σ), 1, 295 ± 19 ka (2σ), 1, 304 ± 9 ka (2σ) for UNK, MNK, and LNK Tuffs respectively; however, even the weighted mean age estimates remain indistinguishable ages for the MNK and LNK Tuffs.

In the almost 20 y since the most recent Nariokotome tuff ages were published, advances in mass spectrometry are such that ^{40}Ar/^{39}Ar age dispersions in feldspar crystals obtained from volcanic tuffs are now commonly reported (e.g., refs. 12, 26, 27, and 40); (Fig. 4 and *SI Appendix*, Fig. S3). Application of the Bayesian statistical approach after Keller, Schoene, and Samperton (25), to such dispersed datasets has gained prominence due to the excellent agreement of age estimates obtained from independent chronometers for example, ^{40}Ar/^{39}Ar on plagioclase and U/Th disequilibrium on Los Chocoyos ash, Central America (26), ^{40}Ar/^{39}Ar on anorthoclase on Turkana Basin tuffs (12), and ^{40}Ar/^{39}Ar on sanidine and U-Pb ID TIMS on zircon from Oxaya Formation ignimbrites, Central Andes (27). The concordance of Bayesian ^{40}Ar/^{39}Ar age estimates for individual pumice samples from each Nariokotome tuff and the analogous composite Bayesian age determinations provides confidence in our age estimates (see additional discussion in *SI Appendix, SI Text, Defining ^{40}Ar/^{39}Ar Age Estimates*). Utilizing this approach, our preferred composite Bayesian age estimate (inclusive of J-uncertainty) for the UNK Tuff is 1,233.1 ± 1.3 ka (2σ) (Fig. 4), which is indistinguishable from the arithmetic mean and weighted mean age provided by McDougall and Brown (4) (based on a single pumice clast; sample 93-1070), but is an order of magnitude more precise.

Similarly, our preferred age of the MNK Tuff based on five of six pumice clasts, is 1,263.4 ± 1.2 ka (2σ; Fig. 4). The older MNK pumice sample (TB23-017-P2; *SI Appendix*, Fig. S3*B*), with a Bayesian eruption age estimate of 1,271.4 ± 2.6 ka, may indicate a failure of this magma fragment to sample the youngest populations of feldspar grains during the eruption. Our preferred age is ~20 ka younger than the arithmetic mean age [1,280.0 ± 64 ka; (4)]; ~35 ka younger than the weighted mean age of MNK Tuff [1,295 ± 19 ka; (4)]. Of the two pumice clasts employed by McDougall and Brown (4) (sample 93-1062A, 93-1062B; Figs. 2 *A–D* and 4 and *SI Appendix*, Fig. S3*B*) we have shown, on the basis of major- and trace-element geochemistry (Fig. 2 *A–D*), and ^{40}Ar/^{39}Ar geochronology (Fig. 4), that sample 93-1062A is an LNK pumice sample that was reworked into the younger MNK Tuff, resulting in an older age estimate for the MNK Tuff layer. This further highlights the importance of forensically examining the geochemistry of pumice glass collected from a given tuff layer while interpreting its ages (further discussed in Section 3.3.1).

Two pumice clasts (93-1062A, TB18-016-P2) from the LNK Tuff yield marginally younger Bayesian eruption ages (after data filtering) relative to the four other LNK pumice clasts. A potential reason for these pumice clasts containing a few (n = 6) feldspar crystals with younger ages could be due to variations in irradiation parameter (J-value uncertainty), analytical bias (e.g., anomalous blanks or hydrocarbon interferences), or geological reasons such as alteration of feldspar grains leading to Ar loss. However, owing to the geochemical similarities of feldspar, pumice glass, and tuff glass for the LNK Tuff, our preferred age of LNK Tuff is given by the composite Bayesian estimate of 1,285.8 ± 1.0 ka (2σ; Fig. 4; n = 149) based on all six pumice clasts where the few (*n* = 2 and 4) anomalously young feldspar grains were excluded from the two younger samples. This age is ~15.5 ka years younger than the arithmetic mean age [1,301.8 ± 50 ka; (4)] and ~20 ka younger

Table 1. Summary table of key geochemical discriminants (fingerprints) for the three Nariokotome tuffs

Tuff Identity	Major Element Oxides	Trace Elements
UNK	Indistinguishable from Mode 2 MNK based on major elements only. **FeO$_T$**: 3.4 – 3.9 wt%, **Al$_2$O$_3$**: 9.9 – 10.9 wt%	**Ti/Zr:** 1.39 ± 0.15, **Ba/Nb:** 4.09 ± 1.8. **La:** 109.0 ± 3.7 ppm, **Zr:** 1,004.9 ± 36.0 ppm
MNK	Mode 1 MNK composition exhibited predominantly by the MNK pumices are distinct in their Al$_2$O$_3$ and FeO$_T$ contents. **Mode 1: FeO$_T$**: 3.8 – 4.5 wt%, **Al$_2$O$_3$**: 10.7 – 11.5 wt%, **Mode 2: FeO$_T$**: 3.1 – 3.7 wt%, **Al$_2$O$_3$**: 9.9 – 10.6 wt%	**Mode 1** (**La:** 90.2 ± 3.5 ppm, **Zr:** 746.2 ± 25.0 ppm) and **Mode 2** (**La:** 123.8 ± 4.0 ppm, **Zr:** 1,126.7 ± 37.4 ppm) **Ti/Zr:** 2.67 ± 0.04 **(Mode 1)**, 1.19 ± 0.14 **(Mode 2)**; **Ba/Nb:** 3.23 ± 0.06 **(Mode 1)**, 4.03 ± 0.48 **(Mode 2)**
LNK	Distinct in Al$_2$O$_3$ and FeO$_T$ contents. **FeO$_T$**: 4.3 – 4.9 wt%, **Al$_2$O$_3$**: 9.2 – 9.8 wt%	**Ti/Zr:** 1.68 ± 0.04, **Ba/Nb:** 0.90 ± 0.07

than the weighted mean age of the LNK Tuff [1, 304 ± 9 ka; (4)], but again, an order of magnitude more precise (Fig. 4).

Potential causes of the feldspar age dispersions for individual pumice clasts have been discussed by Phillips et al. (12). Younger feldspar ages have been attributed to Ar loss, possibly caused by alteration of grains postcrystallization, or irradiation related effects (e.g., variations in neutron flux gradients, self-shielding, recoil artifacts; (12, 41) and references therein). In contrast, older feldspar grains have been attributed to the presence of excess argon that has diffused from the host magma, inherited argon in the early-formed crystals and/or the presence of old K-feldspar antecrysts [(12, 41) and references therein].

High-precision ages from the Nariokotome tuffs also show anorthoclase age distributions spanning timescales of ~ 62 ka (UNK), ~161 ka (MNK) to 208 ka (LNK), respectively (Fig. 4). Since the anorthoclase crystals from the Nariokotome tuffs display remarkably tight compositional clustering across multiple pumice clasts from a given eruptive sequence (Fig. 3), older ^{40}Ar/^{39}Ar ages may represent the retention of (inherited) radiogenic Ar, rather than excess Ar. Similar to the observations by Phillips et al. (12) for other Turkana Basin localities, the range in apparent ages, if due to the retention of inherited radiogenic Ar, could therefore represent the minimum timescales of crystal accumulation during "cold storage" of magma storage' of anorthoclase crystals (i.e., at temperatures ≤470 °C) within silicic magmatic reservoirs for 10 s to 100 s of thousands of years prior to eruption (12, 27, 42). Even if small amounts of excess argon are present, we do not believe it significantly contributes to the older age scatter in our samples. This conclusion aligns with our detailed inspection of the feldspars, which did not reveal melt or fluid inclusions as potential hosts for excess argon (e.g., glass inclusions). Irrespective of the exact cause of the variation of the ages seen in these three tuffs, our high-resolution ^{40}Ar/^{39}Ar geochronology data are able to distinguish, for the first time, the eruption ages of the paleoanthropologically critical Nariokotome tuffs (Fig. 4).

3.3. Insights from High-Resolution ^{40}Ar/^{39}Ar Geochronology and Multielement Geochemistry.

3.3.1. Implications for intra- and interbasin correlation, and age estimates for key archaeological sites. Combining the tephrochronological tools: a) grain-specific major and trace element geochemistry of tuff and pumice glass and major element compositions of feldspars and b) high-resolution ^{40}Ar/^{39}Ar geochronology, it is now possible to provide robust temporal and geochemical identification of the three Nariokotome tuffs. The significance of having unique identifying characteristics improves both intrabasin correlation of these ash layers (i.e., within the Turkana Basin), and the possibility of testing probable correlates of these tuffs in the Konso Formation (Ethiopia) and in Nyabusosi Formation (Uganda), while also providing tighter age constraints for archaeological sites associated with these tephra layers.

3.3.1.1. Intrabasin correlations. The Nariokotome tuffs predominantly outcrop within the Nachukui Formation, West Turkana (Fig. 5*D*) These tuffs have been identified in only one locality (Area 40) on the eastern side of Lake Turkana (Koobi Fora Formation; Fig. 5*E*). Of the two stratigraphic intervals identified in Area 40, the lower layer has previously been identified as the LNK Tuff based on major element compositions of tuff glass (43). Identification of the tuff layer in the upper stratigraphic level proved elusive due to the similar major element geochemistry of the MNK/UNK Tuffs (4) Our study resolves this issue, confirming the identity of the lower stratigraphic interval as a LNK Tuff layer (Figs. 4 and 5 *A*–*C*). Although pumice clast, TB22-100B-P2 was collected from a lag surface (rather than in situ) above the tuff layer, the high-resolution eruption age estimate confirms its LNK affinity and highlights the usefulness of ^{40}Ar/^{39}Ar geochronology as an additional tephrochronological tool. The tuff from the upper stratigraphical level could not be definitively identified the UNK or MNK Tuff (Fig. 5A) (see also ref. 5); however, trace element analyses of tuff glasses, confirmed its identity as the UNK Tuff with its distinct La and Zr abundances and Ti/Zr and Ba/Nb ratios (sample TB22-100B, Fig. 5 *B*, *C*, and *E*). These results have been pivotal in establishing temporal equivalence across the eastern and western sides of Lake Turkana, while also showing the absence of the MNK Tuff in this region.

Having established the trace element fingerprints of the three Nariokotome tuffs, we tested a third layer in Area 40 (sample TB22-100), that exhibits identical major element glass geochemistry to the UNK and MNK Tuffs (Fig. 5*A*). However, the trace element signature shows that this "Unnamed Tuff" does not match either the MNK or UNK Tuffs in terms of glass geochemistry (Fig. 5 *B* and *C*). We did not find any pumice clasts within the layer to determine its age; therefore, its stratigraphic position relative to MNK and UNK Tuff remains unresolved. However, it is notable that this layer could potentially lead to miscorrelation if major element compositions are used as the sole discriminant for the Nariokotome tuffs.

Discrimination of the Nariokotome tuffs is important for constraining the timing of some late Early to Middle Pleistocene archeological sites from Nadung'a [NAD1, NAD2, NAD3, and NAD4; (11, 30, 31)] and Nachukui 6 [NK6; (31)] which are some of the rarely documented late Early to Middle Pleistocene archaeological sites in East Africa, that lie at the base of the Nariokotome Member. For example, a hominid molar tooth [KNM-WT 51261 (11, 31); Fig. 5*D*] was discovered from site NAD 4, which is stratigraphically just above NAD1, 2, and 3 and adjacent to a pumice clast with Silbo Tuff composition, one of the youngest volcanic ash horizons identified in the basin (Fig. 1*C*). The Nadung'a sites have also yielded 6,797 lithic tools, including unconventional Acheulean tools that are uncommon for the time period (30). The ages of the Nadung'a sites have been constrained on the basis of available tephrochronology, primarily through the identification of the UNK and LNK tuffs, and Silbo Tuff (see stratigraphic sections in refs. 11 and 30. Glass major and trace element geochemistry plus ^{40}Ar/^{39}Ar data for the tuff layer in the north bank of Nadung'a river, (samples K88-3287, TB23-019) (Fig. 5 *A*–*D*), reveal that this ash layer is in fact the MNK Tuff, rather than the UNK Tuff [as assigned previously by Maddux, Ward, Brown, Plavcan, and Manthi (11)].

Accurate identification of the LNK Tuff is also important, as it provides a key age constraint for the *H. erectus* left proximal tibia (specimen KNM-WT-19700), located 45 m above the tuff layer in locality NC1, western Turkana (34, 37). The previous age estimate for this fossil was ~1,000 ± 15 ka (29). Our revised age of the LNK Tuff (~15 ka younger), confirms the original age estimate by Brown, Brown, and Walker (29) for KNM-WT-19700. If the age of specimen KNM-WT-19700 is indeed marginally younger, it raises the possibility that it could be contemporaneous with the ~750 ka *H. erectus* molar KNM-WT-51261, found in Nadung'a 4. This molar, discovered near the stratigraphic interval of the Silbo Tuff [dated to 750 ka by McDougall et al. (13)], remains one of the few African hominin fossil fragments from the early Middle Pleistocene (11). Applying the ^{40}Ar/^{39}Ar methodology employed in this investigation to obtain an age for the Silbo Tuff would further help evaluate their potential contemporaneity.

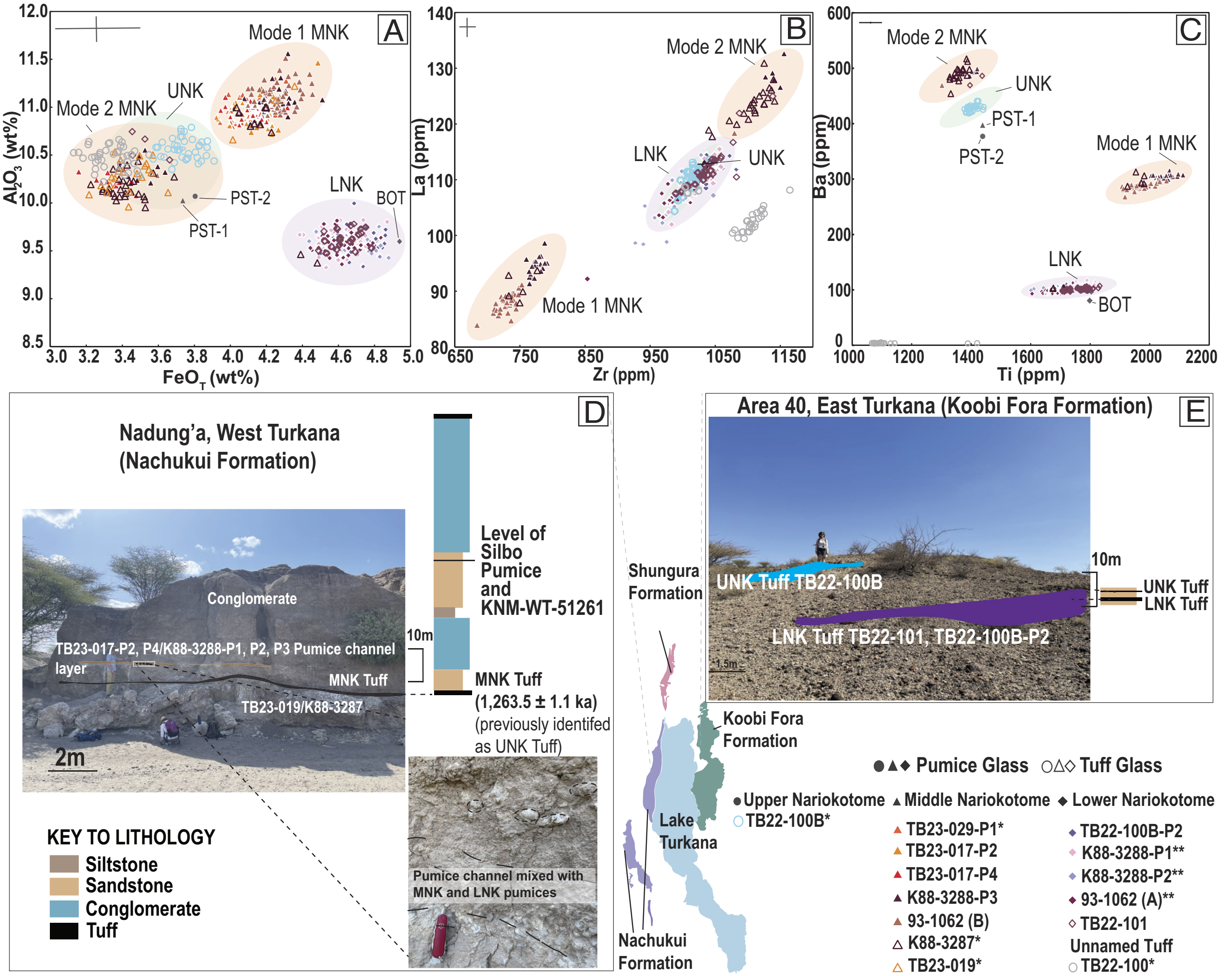

Fig. 5. Tuff correlation of the Nariokotome tuffs between the Nadung'a site, Nachukui Formation (West Turkana), Area 40, Koobi Fora Formation (East Turkana), Konso Tuffs (BOT, PST-1, PST-2; Ethiopia). (*A*–*C*) Geochemical scatter plots showing the established fields of LNK, MNK, and UNK pumice and tuff glass compositions to confirm the identities of samples collected from the above-mentioned sites. Konso Formation tuffs average have been plotted from ref. 21. The fields have been made with tuff and pumice clast geochemistry based on several localities from Nachukui Formation for these three tuffs, excluding the localities mentioned above. (*A*) Al_2O_3 and FeO_T (*B*) La vs. Zr (*C*) Ba vs. Ti. *D*) Photographs showing the locality site Nadung'a and a stratigraphic section which has been modified after (11) with the base tuff, correctly identified as a MNK Tuff rather than a UNK Tuff as previously described. *E*) Photographs of units UNK and LNK Tuffs in Area 40, East Turkana. *: Tuff samples previously misidentified/unidentified due to similar MNK (Mode 2) and UNK major element geochemistry but now correctly identified applying major and trace element geochemistry. **: unidentified reworked LNK pumice samples into the younger MNK Tuff layer.

3.3.1.2. Interbasin correlations. The Nariokotome tuffs are believed to correlate with units outside of the Turkana Basin, specifically in the Konso Formation, Ethiopia, where potentially temporally equivalent strata of the Nariokotome tuffs provide age constraints for young Acheulean stone tools (35). Given the challenges in discriminating the Nariokotome tuffs, the correlations in Konso were termed "probable" by Beyene et al. (35) The speculated equivalent units are UNK = Piso Tuff-2 (PST-2), MNK = Piso Tuff-1 (PST-1), LNK = Bolesche Tuff (BOT) (21, 35), based on tuff glass major and limited bulk XRF/DCP-AES trace element geochemistry. No geochronological data are available for the three Konso tuffs. To test temporal correlation, we plotted major and trace element geochemistry from WoldeGabriel, Hart, Katoh, Beyene, and Suwa (21) for PST-2, PST-1, and BOT together with trace element discriminants from our study for the Nariokotome tuffs (Fig. 5 *A* and *C*). We observe that LNK and BOT have very similar geochemistry, but PST-1 and PST-2 data are offset from the compositions of MNK and UNK Tuffs (Fig. 5*C*). Future work on grain-specific trace element geochemistry on the Konso tuff layers can clarify these discrepancies. Given the probable correlation of the LNK and BOT tuffs, we place a maximum age limit of 1,285 ka (LNK = BOT) for the younger Konso Acheulean toolkit, marginally younger than previously estimated. Similarly, the Kagusa Member of the Nyabusosi Formation, Uganda, known for their early Pleistocene archaeological occurrences is dated between 1,600 to 1,300 ka by correlation of the Morutot and LNK tuffs (28, 36). Since the LNK Tuff is geochemically distinct, the minimum age limit for the archaeological site in Kagusa Member also shifts to a younger estimate of 1,285 ka.

3.3.1.3. Identifying reworked pumices. The upward fluvial reworking of pumices from older stratigraphical levels to younger horizons (24) may lead to erroneous correlations and constraints on the ages of archaeological and paleoanthropological sites. In addition to 93-1062A, a LNK pumice reworked into the MNK Tuff layer (noted in Section 3.2), we recognized several other fluvially reworked older LNK pumice clasts (K88-3288-P1, K88-3288-P2; Fig. 5 *A*–*C*) within a channel in the younger MNK unit at the Nadung'a site. Similar upward reworking of pumices has

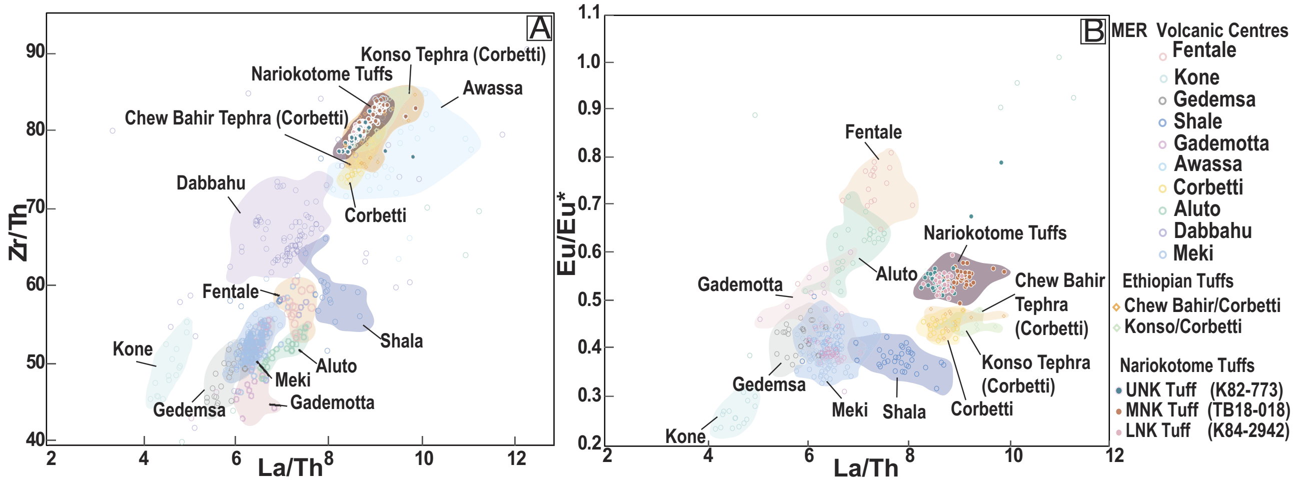

Fig. 6. Geochemical composition of volcanic tephra from late Pleistocene Quaternary calderas in the MER compared with representative data from the three Nariokotome tuffs (UNK represented by K82-773, MNK represented by TB18-018 and LNK represented by K84-2942). (*A*) Zr/Th vs. La/Th (*B*) Eu/Eu* (Eu anomaly) vs. La/Th. Data for Quaternary calderas and distal deposits from Kone, Gedemsa, Gademotta, Shala, Corbetti, Konso Tephra and Chew Bahir Tephra, Fentale (45); Awassa (47); Meki (48); Aluto, Dabbahu (49); Kencherra and Golja Ignimbrites (44).

been noted before in the Okote Tuff Complex (24), but until now has been unrecognized in the Nariokotome Tuff Complex or in the Nadung'a sites. Consequently, we have now provided a more precise and accurate maximum age constraint of the Nadung'a archaeological sites with the identification of this unit as the MNK Tuff at 1,263 ka, ~20 to 30 ka older than published age of MNK (due to reworking of LNK sample 93-106A into the younger MNK unit) and also 30 ka older than the UNK Tuff it was previously assigned as. The maximum age of the Acheulean NK6 site is also given by the MNK Tuff (31) and application of our preferred age means the NK6 site is ~10 ka younger relative than previous estimates (they used a preferred age of 1,270 ka for MNK). Our combined methodology, therefore, highlights the importance in identifying reworked pumices and tuff glass shards, to provide correct age estimates for a given archaeological site.

3.3.2. Magma Source Regions. Previous studies using bulk XRF/Direct Current Plasma Atomic Emission Spectroscopy (DCP-AES) trace element data have speculated that the Turkana Basin tuffs originated from volcanic centers in the central axial rift of the MER, though their exact sources remain unclear (16). The Nariokotome tuffs display negative Eu anomalies in chondrite-normalized REE diagrams and negative Ba, Sr, and Ti anomalies in multielement diagrams (*SI Appendix*, Fig. S3), consistent with fractional crystallization processes in MER rhyolitic systems (20). Recent ^{40}Ar/^{39}Ar geochronology on Plio-Pleistocene ignimbrites in MER suggests temporal overlap between the Nariokotome tuffs and the Golja and Kencherra Ignimbrites (1.20 to 1.30 Ma) (44).

To investigate potential source regions of the Nariokotome tuffs, we compared the trace element ratio signatures (Zr/Th vs La/Th) with proximal volcanic deposits from ten late-Quaternary East African volcanoes as well as the Golja and Kencherra Ignimbrites (Fig. 6). Although modern proximal and distal deposits may not be fully analogous to products of earlier eruptions, they remain the only sources of grain-specific trace element geochemical data currently available from East Africa. As such, they provide a valuable reference for identifying potential petrogenetic links between past and present volcanic systems. The available data show significant overlap between the Nariokotome tuff compositions and those of a younger deposit, the 177 ka Corbetti ignimbrite sample, as well as distal tephra from Konso and Chew Bahir that are thought to also be sourced from Corbetti [(45); Fig. 6*A*]. The Corbetti volcano has been active in the Middle to Late Pleistocene, but a now-buried Pleistocene volcano in Corbetti (Awassa) was active at around ~1.27 to 1.30 Ma (20). While the Golja Ignimbrite might be a more suitable probable proximal deposit, given its precise age estimates, its whole rock trace element geochemistry does not show direct overlap with the Nariokotome tuffs (Fig. 6). Furthermore, the Eu anomaly (Eu/Eu*) of the Nariokotome tuffs (Fig. 6*B* and *SI Appendix*, Fig. S3*B*) is similar, although distinct from, the Corbetti, Golja, and Kencherra Ignimbrites. Temporal changes in Eu anomaly have been attributed to changes in lithospheric thickness (46; in our case the central sector of the MER is an active rift zone), which is plausible given the active rifting of the EARS.

On the evidence available (i.e., the compositional and temporal overlap), we suggest that the Nariokotome tuffs could have tapped a source similar to the modern Corbetti tephra products and/or Awassa. Additionally, the newly suggested Golja Ignimbrite by Franceschini et al. (44) could be a potential proximal deposit. We acknowledge, however, that any potential correlation is hampered by the limited available data, particularly from older early Pleistocene eruptions that may now be buried under late Pleistocene volcanic products. In addition, while each Pleistocene center occupies a distinct cluster in Fig. 6, there is considerable overlap, and until more high-precision geochronological and geochemical studies (including the Golja ignimbrite) are conducted, the correlations between Turkana tuffs and MER volcanic centers can only be hypothesized. Nevertheless, these observations provide a useful framework to guide future source-attribution efforts.

4. Conclusions

We have provided: a) ultra-high-precision, distinguishable ^{40}Ar/^{39}Ar geochronological ages for the previously indistinguishable Nariokotome tuffs; the UNK Tuff at 1,233.1 ± 1.3 ka (± 1.9 ka, including external uncertainties), the MNK Tuff at 1,263.4 ± 1.2 ka (± 1.9 ka) and the LNK Tuff at 1,285.8 ± 1.0 ka (± 2.1 ka), b) shard-specific unique LA-ICP-MS trace element geochemical fingerprints for the three Nariokotome tuffs, that are often otherwise indistinguishable on the basis of major element compositions, a novel application in the area.

The combined methodology of ^{40}Ar /^{39}Ar geochronology and shard-specific major and trace element geochemistry allows the stratigraphical complexities associated with closely spaced ash layers to be resolved, including,

- the identification of tuff horizons and reworking of older eruptive products (pumices) to younger stratigraphic horizons. This approach has highlighted the need to forensically examine the major and trace element geochemistry of pumices, and their host tuff layers, in order to provide accurate and precise age constraints to archaeological/paleontological sites.
- improved age constraints for important archaeological sites within the Nachukui Formation (e.g., Nadung'a and NK6 sites, known for their discovery of early Middle Pleistocene African H. erectus fossil fragments and Acheulean stone tools).
- intrabasinal temporal correlations of the Nariokotome tuffs by identifying LNK and UNK Tuffs (previously unrecognized) in the Koobi Fora Formation (Area 40) and its potential to identify and refine interbasin correlations in other paleoanthropological significant locales throughout East Africa and elsewhere, to establish more robust interbasin correlations between locales, and to correlate distal deposits and proximal products, for example, sourced from calderas in the CMER.

5. Materials and Methods

5.1. Samples and Sample Preparation. Pumice clasts and bulk tuff samples were collected from several sites within the Nachukui Formation, West Turkana (Fig. 1 *A* and *B*). A full list of localities and the sample numbers is given in *SI Appendix, SI Text* and Dataset S1. Several samples (K82-, K84-, K88-, 93- series) were obtained from the University of Utah (Frank Brown) and Australian National University (Ian McDougall) collections; including samples K80-772, K80-773, which were originally used to define the MNK and UNK Tuffs (28) Sample preparation (including washing and separation) of tuff samples, pumice clasts, feldspar separation from pumice clasts (both for geochemical and geochronological analyses) are listed in detail in SI Text and in refs. 12 and 23.

5.2. Analytical Methods.

5.2.1. EPMA. EPMA analyses were conducted using a JEOL JXA-8530F electron microprobe located in the Trace Analysis for Chemical, Earth and Environmental Sciences (TrACEES) Platform at the University of Melbourne. A defocused 10 μm, 5 nA current, with an accelerating voltage of 15 keV electron beam, was used for analysis to minimize volatilization. Fourteen elements were measured. Detection limits, peak and background count times, calibration standards, and X-ray crystals used for different elements are listed in Dataset S2. A atomic number (Z) effect, absorption (A) effect, and fluorescence excitation (F) effect (ZAF) correction method was used to calculate elemental oxide concentrations. Analytical accuracy and precision were monitored using rhyolitic standard VG-568 as a secondary standard (50) during each analytical session. Tuff and pumice glass compositions were recalculated on an anhydrous basis for both tuff and pumice glass as they become variably hydrated postdeposition (5).

5.2.2. LA-ICP-MS. LA-ICP-MS analyses of individual volcanic glass shards extracted from bulk tuff samples, and pumice glass were performed using an Agilent 7700X ICP-MS instrument coupled to an Applied Spectra RESOlution SE 193 nm ArF excimer laser ablation system in the Isotope and Trace Element Geochemistry Laboratory at the University of Melbourne. The instrument and acquisition parameters are summarized in detail in ref. 23 (*SI Appendix, SI Text, Extended Methods*). A traverse ablation strategy, previously validated by Samim et al. (19), with a repetition rate of 5 Hz and a beam diameter of 20 μm was used for the acquisition of data for thirty trace elements. ^{29}Si was used as an internal standard and Si values for unknowns were acquired by EPMA (nonhydrous Si concentration of tuff and pumice glass) before ablation. Data were reduced using NIST612 as a calibration standard using Iolite v.4 software (https://iolite.xyz). Secondary reference materials used were MPI-DING certified natural reference materials ATHO-G (rhyolite standard) and StHs6/80-G (andesite standard), and our in-house reference sample K84-2942 (42TG; details in ref. 23). Data were reduced, and the results underwent an offline 42TG internal correction. Correction factors from 42TG were acquired from analyses of individual glass shards that were run in the same session as the unknowns.

5.2.3. ^{40}Ar/^{39}Ar Geochronology. Cleaned anorthoclase crystals were packed in Al-foil packets which contained subpackets of Fish Canyon Tuff sanidine (FCTs) grains as flux monitors and sent for irradiation to the CLICIT nuclear reactor facility in Oregon State University TRIGA reactor. Samples were irradiated in three batches, UM#94 (6 MWh), UM#99 (6 MWh), and UM#101 (4 MWh). ^{40}Ar/^{39}Ar analyses were carried out in the Noble Gas Laboratory at the University of Melbourne using multicollector Thermo Fisher Scientific ARGUSVI (UM#94) and ARGUSVI+ (UM#99 and UM#101) mass spectrometers, linked to Photon Machines Fusions 10.6 CO_2 lasers and stainless-steel extraction lines. A summary of the instrument detectors and interference corrections for Ar isotope peaks, can be found in Dataset S7 and are described in detail by Phillips and Matchan (51) and Phillips et al. (12). Procedures for sample and standard analyses are outlined in *SI Appendix*, SI Text.

The total ^{40}K decay constant of $5.463 (\pm 0.107) \times 10^{-10}$ y^{-1} (52) and an age of 28.176 ± 0.011 (± 0.023) Ma (53), for FCTs were used to calculate apparent ages for individual analyses. All ages are reported at the 2σ level, unless otherwise stated. External uncertainties (uncertainties from the decay constant and age of FCTs) are only incorporated and reported for the final ages.

5.3. Data Treatment. Analyses with a low ^{40}Ar or ^{39}Ar yield (i.e., <25 fA) or with low radiogenic Ar (^{40}Ar* < 70%) were discarded. After data filtering, it is evident that all samples have positively skewed age distributions. Such dispersed ^{40}Ar/^{39}Ar ages within an individual sample precludes calculating a simple weighted mean to provide an eruption age for a given sample (on statistical grounds). Following the work of Phillips et al. (12) and van Zalinge et al. (27), we use a Bayesian statistical approach [after Keller, Schoene, and Samperton (25) and modified by van Zalinge et al. (27)] to calculate eruption age estimates for age distributions obtained from different feldspar grains recovered from an individual pumice clast. Phillips et al. (12) evaluated alternative ways (e.g., normalized median absolute deviation, low MSWD weighted mean, weighted mean, normality test, and goodness-of-fit filter) to evaluate dispersed exponential ^{40}Ar/^{39}Ar datasets, but concluded that the Bayesian statistical approach yielded the most concordant results from multiple pumice clasts obtained from a single tuff layer (*SI Appendix, SI Text, Defining 40Ar/39Ar Age Estimates*). We have also calculated a composite Bayesian age for the combined dataset of feldspar ages from pumices collected from a single tuff. This is not a strictly hierarchical approach to uncertainty estimation. However, we found that the J-value uncertainty has a minimal contribution to individual feldspar analyses, with intersample weighted Bayesian age estimates being indistinguishable from combined Bayesian ages and insensitive to inclusion or exclusion of J-value uncertainty. Ages from McDougall and Brown (4) have been recalculated to the decay constant of Min, Mundil, Renne, and Ludwig (52) and FCT age of 28.176 ± 0.011 (± 0.023) Ma (53). We then calculated an arithmetic mean age and uncertainties as preferred by McDougall and Brown (4) for the eruption age estimates of the three Nariokotome tuffs.

Data, Materials, and Software Availability. Supporting dataset have been deposited in AusGeochem (10.58024/AGUM5B34174D) (38). All other data are included in the article and/or supporting information.

ACKNOWLEDGMENTS. This study could not have been undertaken without the samples that were received from the late Frank Brown's University of Utah collection and the late Ian McDougall's Australian National University collection. Hilary Sale and Francis Ikai Ekai from the Turkana Basin Institute are thanked for their assistance during field work and sample collection related to this project. This work was performed in part with sample preparation and EPMA facilities available in the Trace Analysis for Chemical, Earth and Environmental Sciences Platform at the University of Melbourne (UoM). Graham Hutchinson and Dr. Ling Chung are thanked for assisting with microprobe analyses and sample preparation. Dr. Alan Greig from UoM is also thanked for their assistance in LA-ICP-MS trace element geochemistry. Dr. Erin Matchan, Ashley Savelkouls and Stan Szczepanski from UoM are also thanked for their support in field work and ^{40}Ar/^{39}Ar geochronology analysis respectively. We also thank T. Cerling for efficient editorial handling. The manuscript has benefited from thoughtful reviews by C. Feibel, W. Hart, and an anonymous reviewer. This study was supported financially by Australian Research Council Discovery Grant DP180101412 to D.P. and J.H.; Turkana Basin Institute

Research Continuity Awards granted to S.S., H.D., D.P., and J.H.; UoM Graduate Research Scholarship (Melbourne Research Scholarship) awarded to S.S. The Melbourne ^{40}Ar/^{39}Ar laboratory receives ongoing operational support under the AuScope programme of the National Collaborative Research Infrastructure Strategy (https://www.education.gov.au/ncris; https://www.auscope.org.au).

Author affiliations: [a]School of Geography, Earth and Atmospheric Sciences, Faculty of Science, The University of Melbourne, Parkville, Melbourne, VIC 3010, Australia

Author contributions: S.S., D.P., and J.H. designed research; S.S., H.D., D.P., and J.H. performed research; S.S., H.D., D.P., and J.H. contributed new reagents/analytic tools; S.S., H.D., D.P., and J.H. analyzed data; and S.S., H.D., D.P., and J.H. wrote the paper.

The authors declare no competing interest.

1. B. V. Alloway, D. J. Lowe, G. Larsen, P. A. R. Shane, J. A. Westgate, "Quaternary Stratigraphy|Tephrochronology" in *Encyclopedia of Quaternary Science*, S. A. Elias, Ed. (Elsevier, 2013), 10.1016/b978-0-444-53643-3.00058-3, pp. 277–304.
2. D. J. Lowe, Tephrochronology and its application: A review. *Quat. Geochronol.* **6**, 107–153 (2011).
3. I. McDougall, F. H. Brown, Geochronology of the pre-KBS tuff sequence, Omo Group, Turkana Basin. *J. Geol. Soc.* **165**, 549–562 (2008).
4. I. McDougall, F. H. Brown, Precise 40Ar/39Ar geochronology for the upper Koobi Fora Formation, Turkana basin, northern Kenya. *J. Geol. Soc.* **163**, 205–220 (2006).
5. F. H. Brown, B. Haileab, I. McDougall, Sequence of tuffs between the KBS tuff and the Chari tuff in the Turkana Basin, Kenya and Ethiopia. *J. Geol. Soc.* **163**, 185–204 (2006).
6. J. M. Harris, F. H. Brown, M. G. Leakey, A. C. Walker, R. E. Leakey, Pliocene and Pleistocene hominid-bearing sites from west of Lake Turkana, Kenya. *Science* **239**, 27–33 (1988).
7. C. S. Feibel, A geological history of the Turkana Basin. *Evol. Anthropol.* **20**, 206–216 (2011).
8. B. Wood, M. Leakey, The Omo-Turkana Basin fossil hominins and their contribution to our understanding of human evolution in Africa. *Evol. Anthropol.* **20**, 264–292 (2011).
9. C. J. Lepre *et al.*, An earlier origin for the Acheulian. *Nature* **477**, 82–85 (2011).
10. S. Harmand *et al.*, 3. 3-million-year-old stone tools from Lomekwi 3, West Turkana, Kenya. *Nature* **521**, 310–315 (2015).
11. S. D. Maddux, C. V. Ward, F. H. Brown, J. M. Plavcan, F. K. Manthi, A 750, 000 year old hominin molar from the site of Nadung'a, West Turkana. *J. Hum. Evol.* **80**, 179–183 (2015).
12. D. Phillips *et al.*, 40Ar/39Ar eruption ages of Turkana Basin tuffs: Millennial-scale resolution constrains palaeoclimate proxy tuning models and hominin fossil ages. *J. Geol. Soc.* **180**, jgs2022-2171 (2023).
13. I. McDougall *et al.*, New single crystal40Ar/39Ar ages improve time scale for deposition of the Omo Group, Omo-Turkana Basin, East Africa. *J. Geol. Soc.* **169**, 213–226 (2012).
14. A. Nutz, M. Schuster, X. Boës, J.-L. Rubino, Orbitally-driven evolution of Lake Turkana (Turkana Depression, Kenya, EARS) between 1.95 and 1.72 Ma: A sequence stratigraphy perspective. *J. Afr. Earth Sci.* **125**, 230–243 (2017).
15. J. d. Heinzelin, The Omo group–Archives of the International omo research expedition. *Annales du Musée Royal de l'Afrique Centrale Tervuren, Belgique, série* **8** (1983).
16. T. Cerling, F. Brown, Tuffaceous marker horizons in the Koobi Fora region and the Lower Omo Valley. *Nature* **299**, 216–221 (1982).
17. F. Brown, T. Cerling, Stratigraphical significance of the Tulu Bor tuff of the Koobi Fora formation. *Nature* **299**, 212–215 (1982).
18. T. Cerling, B. Cerling, G. Curtis, R. Drake, F. Brown, Preliminary correlations between the Koobi Fora and Shungura formations, East Africa. *Nature* **279**, 118–121 (1979).
19. K. Fontijn *et al.*, Contrasting styles of post-caldera volcanism along the Main Ethiopian Rift: Implications for contemporary volcanic hazards. *J. Volcanol. Geotherm. Res.* **356**, 90–113 (2018).
20. G. Woldegabriel, J. L. Aronson, R. C. Walter, Geology, geochronology, and rift basin development in the central sector of the Main Ethiopia Rift. *Geol. Soc. Am. Bull.* **102**, 439–458 (1990).
21. G. WoldeGabriel, W. K. Hart, S. Katoh, Y. Beyene, G. Suwa, Correlation of Plio-Pleistocene tephra in Ethiopian and Kenyan rift basins: Temporal calibration of geological features and hominid fossil records. *J. Volcanol. Geotherm. Res.* **147**, 81–108 (2005).
22. C. J. Ebinger, M. Casey, Continental breakup in magmatic provinces: An Ethiopian example. *Geology* **29**, 527–530 (2001).
23. S. Samim, H. Dalton, J. Hergt, A. Greig, D. Phillips, An improved methodology for high-resolution LA-ICP-MS trace-element fingerprinting of tephra layers: Insights from the Upper and Lower Nariokotome Tuffs, Turkana Basin, Kenya. *Chem. Geol.* **660** (2024).
24. F. H. Brown, C. S. Feibel, Stratigraphical notes on the Okote tuff complex at Koobi Fora, Kenya. *Nature* **316**, 794–797 (1985).
25. C. B. Keller, B. Schoene, K. M. Samperton, A stochastic sampling approach to zircon eruption age interpretation. *Geochem. Perspect. Lett.* 31–35 (2018), 10.7185/geochemlet.1826.
26. A. Baudry *et al.*, A bayesian age from dispersed plagioclase and zircon dates in the Los Chocoyos ash, Central America. *Earth Planet. Sci. Lett.* **643** (2024).
27. M. E. van Zalinge *et al.*, Timescales for pluton growth, magma-chamber formation and super-eruptions. *Nature* **608**, 87–92 (2022).
28. J. Harris, F. Brown, M. Leakey, Stratigraphy and paleontology of the Nachukui Formation, Lake Turkana region, Kenya. *Contrib. Sci.* **399**, 1–128 (1988).
29. B. Brown, F. H. Brown, A. Walker, New hominids from the Lake Turkana basin. Kenya. *J. Hum. Evol.* **41**, 29–44 (2001).
30. A. Delagnes *et al.*, Interpreting pachyderm single carcass sites in the African Lower and Early Middle Pleistocene record: A multidisciplinary approach to the site of Nadung'a 4 (Kenya). *J. Anthropol. Archaeol.* **25**, 448–465 (2006).
31. X. Boes *et al.*, Aridity, availability of drinking water and freshwater foods, and hominin and archeological sites during the late Pliocene-early Pleistocene in the western region of the Turkana Basin (Kenya): A review. *J. Hum. Evol.* **186**, 103466 (2024).
32. M. Kibunjia, H. Roche, F. H. Brown, R. E. Leakey, Pliocene and Pleistocene archeological sites west of Lake Turkana. *J. Hum. Evol.* **23**, 431–438 (1992).
33. C. J. Lepre, R. L. Quinn, Aridification and orbital forcing of eastern African climate during the Plio-Pleistocene. *Glob. Planet. Change* **208** (2022).
34. S. Katoh *et al.*, Chronostratigraphy and correlation of the Plio-Pleistocene tephra layers of the Konso Formation, southern Main Ethiopian Rift. *Quat. Sci. Rev.* **19**, 1305–1317 (2000).
35. Y. Beyene *et al.*, The characteristics and chronology of the earliest Acheulean at Konso, Ethiopia. *Proc. Natl. Acad. Sci. U.S.A.* **110**, 1584–1591 (2013).
36. I. Mesfin, P.-J. Texier, Prepared core technology from the early Pleistocene site of Nyabusosi 18, Uganda. *J. Archaeol. Sci. Rep.* **46** (2022).
37. C. S. Feibel, F. H. Brown, I. McDougall, Stratigraphic context of fossil hominids from the Omo group deposits: Northern Turkana Basin, Kenya and Ethiopia. *Am. J. Phys. Anthropol.* **78**, 595–622 (1989).
38. S. Samim, H. Dalton, D. Phillips, J. Hergt, Data from "A tale of the Nariokotome tuffs, Turkana Basin, Kenya: High-resolution Ar-Ar geochronology, major and LA-ICP-MS trace element geochemistry of Upper, Middle and Lower Nariokotome Tuffs." Earthbank. https://app.ausgeochem.org/doi/10.58024/AGUM5B34174D#/. Deposited 25 November 2024.
39. K. R. Ludwig, User's manual for Isoplot 3.75: A geochronological toolkit for Microsoft Excel. *Berkeley Geochronol. Center Spl. Publ.* **5**, 75 (2012).
40. N. L. Andersen, B. R. Jicha, B. S. Singer, W. Hildreth, Incremental heating of Bishop Tuff sanidine reveals preeruptive radiogenic Ar and rapid remobilization from cold storage. *Proc. Natl. Acad. Sci. U.S.A.* **114**, 12407–12412 (2017).
41. A. J. Schaen *et al.*, Interpreting and reporting 40Ar/39Ar geochronologic data. *GSA Bull.* **133**, 461–487 (2020).
42. M. P. Castellanos Melendez *et al.*, Explosive volcanism of Piton des Neiges (Reunion Island) and excess age dispersion in sanidine: Insights into magma chamber processes in a hotspot setting. *Chem. Geol.* **632** (2023).
43. P. N. Gathogo, F. H. Brown, Stratigraphy of the Koobi Fora Formation (Pliocene and Pleistocene) in the Ileret region of northern Kenya. *J. Afr. Earth Sci.* **45**, 369–390 (2006).
44. Z. Franceschini *et al.*, Pulsatory volcanism in the Main Ethiopian Rift and its environmental consequences. *Commun. Earth Environ.* **5**, 568 (2024).
45. C. M. Vidal *et al.*, Geochronology and glass geochemistry of major Pleistocene eruptions in the Main Ethiopian Rift: Towards a regional tephrostratigraphy. *Quat. Sci. Rev.* **290** (2022).
46. M. Tang, W.-Q. Ji, X. Chu, A. Wu, C. Chen, Reconstructing crustal thickness evolution from europium anomalies in detrital zircons. *Geology* **49**, 76–80 (2020).
47. C. M. Martin-Jones *et al.*, Glass compositions and tempo of post-17 ka eruptions from the Afar Triangle recorded in sediments from lakes Ashenge and Hayk. *Quat. Geochronol.* **37**, 15–31 (2017).
48. A. Z. Tadesse *et al.*, Pre-eruptive storage conditions and magmatic evolution of the Bora-Baricha-Tullu Moye volcanic system, Main Ethiopian Rift. *Lithos* **442–443** (2023).
49. W. Hutchison *et al.*, The evolution of magma during continental rifting: New constraints from the isotopic and trace element signatures of silicic magmas from Ethiopian volcanoes. *Earth Planet. Sci. Lett.* **489**, 203–218 (2018).
50. E. Jarosewich, J. A. Nelen, J. A. Norberg, Reference samples for electron microprobe analysis*. *Geostand. Newsl.* **4**, 43–47 (1980).
51. D. Phillips, E. L. Matchan, Ultra-high precision 40Ar/39Ar ages for Fish Canyon Tuff and Alder Creek Rhyolite sanidine: New dating standards required? *Geochim. Cosmochim. Acta* **121**, 229–239 (2013).
52. K. Min, R. Mundil, P. R. Renne, K. R. Ludwig, A test for systematic errors in 40Ar/39Ar geochronology through comparison with U/Pb analysis of a 1.1-Ga rhyolite. *Geochim. Cosmochim. Acta* **64**, 73–98 (2000).
53. D. Phillips, E. L. Matchan, H. Dalton, K. F. Kuiper, Revised astronomically calibrated 40Ar/39Ar ages for the Fish Canyon Tuff sanidine–Closing the interlaboratory gap. *Chem. Geol.* **597** (2022).